# Measurement of Gamow-Teller strength for $^{127}$I as a solar neutrino detector

M. Palarczyk,* J. Rapaport, and C. Hautala
*Ohio University, Athens, Ohio 45701*

D. L. Prout
*Department of Physics, Kent State University, Kent, Ohio 44242*

C. D. Goodman, I. J. van Heerden,† J. Sowinski, G. Savopulos, and X. Yang‡
*Indiana University Cyclotron Facility, Bloomington, Indiana 47405*

H. M. Sages,§ R. Howes, R. Carr, and M. Islam
*Ball State University, Muncie, Indiana 47306*

E. Sugarbaker and D. C. Cooper‖
*The Ohio State University, Columbus, Ohio 43210*

K. Lande
*University of Pennsylvania, Philadelphia, Pennsylvania 19104*

B. Luther
*Concordia College, Moorhead, Minnesota 56562*

T. N. Taddeucci
*Los Alamos National Laboratory, Los Alamos, New Mexico 87545*
(Received 28 April 1998)

Gamow-Teller transition strengths obtained in the $^{127}$I$(p,n)^{127}$Xe reaction studied at 94, 159, and 197 MeV incident proton energies are presented, and used to evaluate the efficiency of $^{127}$I as a solar neutrino detector. Excitation of the $J^{\pi}=(3/2)^{+}$ first excited state at $E_x=0.125$ MeV in $^{127}$Xe, sensitive to $^{7}$Be solar neutrinos, is evaluated. The sum of Gamow-Teller strength up to particle emission threshold and up to 20 MeV excitation energy are also reported. This paper also provides a new measurement of the Coulomb displacement energy $\Delta E_c$, the excitation energy of the isobaric analog state, and the centroid of the Gamow-Teller resonance in $^{127}$Xe. [S0556-2813(99)02101-9]

PACS number(s): 26.65.+t, 25.40.Kv, 24.10.Eq

## I. INTRODUCTION

The observed flux of neutrinos emitted by nuclear fusion reactions in the solar core are considerably less than predicted by models of the solar interior. This discrepancy has been observed by each of the five operating solar neutrino experiments: the chlorine detector in the Homestake Mine, the Kamiokande and Superkamiokande detectors in Japan, and the two gallium detectors GALLEX and SAGE. From analysis of the combined results it appears that the highest energy component of the solar neutrino emission, that due to the decay of $^{8}$B, is about half of that predicted, the middle component, that in the 1 MeV range, due to the decay of $^{7}$Be, the *pep* reaction, and the CNO cycle, is almost completely absent and the lowest component, that below 0.5 MeV due almost entirely to *p-p* fusion, is observed at approximately the predicted intensity.

The most dramatic and startling effect, the almost complete absence of electron neutrinos in the 1 MeV range, is obtained by subtracting the $^{8}$B neutrino flux determined by the Superkamiokande detector from the observations of the Homestake chlorine detector. Clearly, this result should be verified by another detector with the same range of sensitivity. That is, we need another electron neutrino detector that is sensitive to neutrinos in the 1 MeV range, but has a threshold above the *p-p* neutrino range so that it is not overwhelmed by the large flux of these low energy neutrinos.

In 1988 Haxton [1] pointed out that $^{127}$I meets the above criteria. The nuclear reaction involved in the process, $^{127}$I $(\nu_e,e)^{127}$Xe $(\tau_{1/2}=36.4$ d), yields $^{127}$Xe, a noble-gas product, that can be recovered with techniques similar to the recovery of $^{37}$Ar [2] produced in the reaction $^{37}$Cl$(\nu_e,e)^{37}$Ar $(\tau_{1/2}=35.0$ d). The technology of a radiochemical version of an iodine solar neutrino detector closely follows that of the chlorine detector and has been demon-

*Permanent address: Henryk Niewodniczański Institute of Nuclear Physics, 31-342 Kraków, Poland.
†Permanent address: University of the Western Cape, Bellville, South Africa.
‡Present address: Motorola Inc., Arlington Heights, IL 60004.
§Present address: IIT Research Institute, Annapolis, MD 21401.
‖Present address: MIT/Lincoln Laboratory, Lexington, MA 02173.

 

strated in a pilot $^{127}$I detector operated at the University of Pennsylvania [3].

The critical issue for an iodine solar neutrino detector is the determination of the cross section as a function of energy for the $^{127}\mathrm{I}(\nu_e,e)^{127}\mathrm{Xe}$ reaction. In order to determine the high energy part of this cross section, Cleveland and collaborators have placed an $^{127}$I detector near the Los Alamos Meson Physics Facility (LAMPF) proton beam stop and have measured the total absorption cross section for $\mu^+$ neutrinos produced by $\pi$ decay in the proton beam stop [4]. This neutrino spectrum is similar to that produced by a supernova and extends up to a neutrino energy of 53 MeV. Production of a MCi source of $^{37}$Ar that will give a monoenergetic 814 keV electron neutrinos is now beginning in Russia [3]. This source will permit measurement of the response of an iodine detector to $^{7}$Be electron neutrinos.

In his paper, Haxton [1] pointed out that for the proposed $^{127}$I detector, the capture cross section for $^{7}$Be neutrinos ($\epsilon_\nu = 0.862$ MeV) should depend only on the strength of the Gamow-Teller (GT) transition between the ground state (g.s.) of $^{127}$I, $J^\pi = 5/2^+$, and the 0.125 MeV excited state in $^{127}$Xe, $J^\pi = 3/2^+$. The higher energy solar neutrinos from $^{8}$B can produce $^{127}$Xe atoms by exciting many transitions to excited states below the neutron breakup threshold (particle emission threshold) at 7.223 MeV excitation energy [5].

Haxton [1] argues that if the GT transition to the 0.125 MeV excited state has a $\log(ft)$ greater or smaller than 5.10 [value for $^{37}\mathrm{Ar}(EC)^{37}\mathrm{Cl}$], the $^{127}$I detector would have greater or lower sensitivity to $^{7}$Be neutrinos. Also, the ratio for the capture of $^{8}$B neutrinos to that of $^{7}$Be neutrinos will depend on the Fermi (F) and GT strength below the particle emission threshold in each detector. The comparison of the resulting $^{127}$I neutrino capture data with the $^{37}$Cl results could provide better information about the flux of $^{7}$Be neutrinos emitted by the Sun.

It has been empirically shown that data obtained from zero-degree $(p,n)$ charge exchange cross sections, measured at incident energies between 100 and 200 MeV, may be used to deduce GT strengths in nuclei. This technique has been used for $^{37}$Cl and $^{71}$Ga nuclei [6,7]. In this paper we report a measurement of the Gamow-Teller strength distribution from the $^{127}$I to excited states in $^{127}$Xe as determined from $^{127}\mathrm{I}(p,n)^{127}\mathrm{Xe}$ reaction.

The first excited state at 0.125 MeV is the lowest state in $^{127}$Xe that can be excited by a GT transition. Several other states below 1 MeV have been observed by Champagne *et al.* [8] in $^{127}\mathrm{I}(^3\mathrm{He},t)^{127}\mathrm{Xe}$ and by Lonnroth *et al.* [9] in a low energy $^{127}\mathrm{I}(p,n\gamma)^{127}\mathrm{Xe}$ reaction. Eleven excited states below 1 MeV have been assigned [10] a $J^\pi$ of $(3/2)^+$,$(5/2)^+$, or $(7/2)^+$ and might show GT strength from the $^{127}$I g.s. However, only the 0.125 MeV state can be excited by neutrinos from the $^{7}$Be decay chain ($\epsilon_\nu = 862$ keV). To determine the GT strength to the 0.125 MeV state with the $(p,n)$ reaction an energy resolution of better than 200 keV is required, since the next possible GT state is only 197 keV higher.

The first measurement of the $^{127}\mathrm{I}(p,n)$ charge exchange reaction at intermediate energy was performed by Sugarbaker [11] at the Indiana University Cyclotron Facility (IUCF) utilizing the beam swinger. This author used a beam energy $T_p = 120$ MeV and a 29.8 mg/cm$^2$ thick target made of calcium iodine. The neutron detectors were oriented longitudinally, with their long direction along the neutron beam (so-called spectroscopy mode with time compensation) and the neutron detector station was located at 121 m from the target. The achieved energy resolution was only 320 keV full width at half maximum (FWHM). The low excitation energy range of the observed neutron spectrum at $\theta_{\mathrm{lab}} = 0^\circ$ showed almost a featureless character, with no visible peak comparable, for instance, to that seen in $^{71}$Ge [7]. The higher excitation part was dominated by the isobaric analog state (IAS) riding on a broad GT structure, located between $E_x = 12$ and 13 MeV. By using the energy dependence of the ratio of the intrinsic spin flip (Gamow-Teller) $\hat{\sigma}_{\mathrm{GT}}$ to the intrinsic non-spin-flip (Fermi) $\hat{\sigma}_F$ unit cross sections,

$$R^2 = \frac{\hat{\sigma}_{\mathrm{GT}}}{\hat{\sigma}_F} = \left[\frac{T_p}{E_0}\right]^2, \tag{1}$$

and using $E_0 = (50 \pm 5)$ MeV, the author estimated the following GT strength values. In the above equation, the unit cross section is defined as the GT (F) cross section in mb/sr per unit GT (F) strength. In these units, the neutron decay has a GT strength of 3. The integral from $E_x = 0$ MeV up to the particle emission threshold was estimated to be $(3.2 \pm 0.1)$ unit GT and over the excitation energy, including the lowest four excited states in $^{127}$Xe that may show GT strength, to be $(0.028 \pm 0.003)$ unit GT. The uncertainties in the above values are only statistical. Because of the achieved resolution, they estimated the upper limit for the GT strength for the first excited state to be half of the observed strength or 0.014 unit GT. A nonstatistical uncertainty of $\pm 20\%$ should be included in the above empirical values to reflect the uncertainty of 10% in the assumed value of $E_0$.

The previous experiment [11] failed to provide more precise information about the distribution of the GT strength in the low excitation energy states of $^{127}$Xe. In particular the first excited state was not isolated. Therefore we decided to repeat this experiment at IUCF using an apparatus characterized by high resolution and high background suppression.

In this paper we present $\theta_{\mathrm{lab}} = 0^\circ$ results for the $^{127}\mathrm{I}(p,n)^{127}\mathrm{Xe}$ reaction obtained at beam energies of 94, 159, and 197 MeV. In particular, evidence for the excitation of the 0.125 MeV state in $^{127}$Xe as well as values for the GT strength observed up to the particle emission threshold and up to 20 MeV of excitation in $^{127}$Xe is presented.

## II. EXPERIMENTAL METHOD

To achieve a good energy resolution in a time-of-flight measurement a long flight path and good time resolution are required. However, extending the flight path usually reduces the peak-to-background ratio in the neutron detector. To improve the signal-to-background ratio one can use a neutron polarimeter, where a coincidence condition is required between two neutron detectors (polarimetry mode). The polarimetry mode is very efficient in suppressing the background; however, it also reduces the neutron detection efficiency, which is already typically low.

At IUCF a new neutron polarimeter, INPOL, has recently been installed at a fixed distance of 159 m from the target. Complete information about this polarimeter may be found in Ref. [12]. Briefly, INPOL consists of two front detector planes (analyzer planes) and two back detector planes (catcher planes), separated by a charged particle veto plane. To reject charge particles coming from the target a large veto detector is placed in front of the analyzer planes. Each 1.0 m$\times$1.0 m$\times$0.1 m plane is divided into ten individual detector cells. Each cell operates as a separate detector and provides position information along its length. Requiring a coincidence between the analyzer planes and the catcher planes suppresses the background from cosmic radiation and additional information is obtained from the kinematics of the interplane scattering. When the neutron detectors operate in the spectroscopy mode, background is usually suppressed by raising the energy threshold on the detector analog output. This procedure makes the response of the neutron detector strongly energy dependent, and final spectra require a careful correction for this energy-dependent efficiency. In contrast to the spectroscopy mode, the polarimetry mode allows low neutron energy thresholds. Another tool available in the polarimetry mode is the velocity ratio. From the time of flight of the incoming neutron to the analyzer planes and from the conversion location in the catcher planes one can calculate the interplane time of flight and form a ratio of measured and expected velocities of the scattered particle. The expected velocity is calculated using kinematics for $n$-$p$ scattering. This ratio yields unity for scattering from the H component of the scintillator material. Other event types with kinematics or timing not matched to $n$-$p$ scattering will yield higher or lower values for this ratio, and thus can be discriminated against. In this way one can eliminate slow neutrons from previous beam bursts (known as pulse selection feed throughs) and suppress signals from cosmic-ray showers and other background. The cyclotron beam pulses are separated by about 30 ns. Time-of-flight experiments require longer pulse separations. In the present case we removed several beam pulses from the primary proton beam to achieve pulse separations of about 300 ns. The unwanted pulses are removed by a beam buncher and chopper, but they may not be completely suppressed. Slow neutrons from previous pulses and poorly suppressed pulses can increase the background at the neutron detector. The velocity ratio offers an effective way to suppress this form of background.

Data for this experiment were collected using the INPOL detector in polarimetry mode at zero degrees. Three incident energies were selected: 94.1, 159.1, and 197.4 MeV, with pulse selections of 1:10, 1:12, and 1:3, respectively. At both the low and medium incident energies this allowed us to study an excitation range well above the IAS state in $^{127}$Xe state and ensured a wide time separation between proton bursts. The lowest input proton energy was chosen to ensure a good energy resolution. The lower the incident proton energy the greater becomes the time dispersion between outgoing neutrons traveling to the detector with different energies. Therefore, for a given time resolution of the detection system the better is the achieved energy resolution. During a test run prior to the main measurement, an energy resolution of $\Delta E \sim 200$ keV at an incident beam energy of $T_p \sim 100$ MeV was achieved. The 159.1 MeV input energy was selected because this collaboration has previously carried out $(p,n)$ experiments at this energy to measure GT transition strengths [13]. Short runs at the highest incident energy were collected in order to compare specific spectrum integrals to those obtained at the lower incident energies, rather than to study low lying excited states. Therefore we will discuss experimental conditions at the lower (94.1 MeV) and medium (159.1 MeV) incident energies in greater detail.

Usually in a high resolution neutron experiment two beam related factors are critical: the cyclotron timing and the energy spread across the target. In this experiment, the estimated time spread in the beam, based on measurements made with a fast plastic-scintillator telescope located close to the target, was $\sim 350$ ps at low beam energy and $\sim 500$ ps at medium beam energy. The intrinsic time resolution of the INPOL polarimeter determined from cosmic-ray muon tracks is on the order of 300 ps. The beam-related factors depend on how the cyclotron has been tuned. Using narrow energy-defining slits reduces the energy spread across the target at the expense of beam intensity. At the incident energy of $T_p = 159.1$ MeV the estimated energy spread was smaller than 150 keV. To achieve the long range time stability critical for experiments with low luminosity, one must track small time fluctuations of the beam with respect to the cyclotron radio frequency. Both the cyclotron crew and the experimenters invested considerable effort to achieve a good and stable beam intensity of about 300 nA at 94.1 MeV and about 100 nA at 159.1 MeV. The total collection time of ''good events'' was $\sim 8000$ min at lower energy and $\sim 2000$ min at medium energy.

The beam stability and overall resolution were periodically checked by using the $^7$Li$(p,n)^7$Be reaction at 0 °. The two lowest states of $^7$Be, the ground state with $J^\pi = 3/2^-$ and the first excited state with $J^\pi = 1/2^-$, are separated by 0.429 MeV. The separation between the two states in spectra recorded with a thin $^7$Li target ($\sim 20$ mg/cm$^2$) served as a useful monitor of the overall experimental performance.

### A. Achieved energy resolution

The INPOL polarimeter offers two triggers to measure the neutron time of flight. The first is the NN (neutron-neutron) trigger, where incoming neutrons are registered in the analyzer planes followed by neutron scattering into the catcher planes. The second, the NP (neutron-proton) trigger, occurs when in the analyzer planes most of the incident neutron momentum is transferred to a proton, which is then scattered into the catcher planes. The advantage of the second trigger is a 100% detection efficiency in the catcher planes and significant improvement in the measurement of the interplane time and flight path. The latter makes the velocity cut more efficient. Because of the range of recoiling protons, the NP trigger is useful only at the higher input energy. It also requires a larger efficiency correction.

Figure 1 present zero-degree spectra obtained in the $^7$Li$(p,n)^7$Be reaction at both lower energies. In Fig. 1 panels (A) and (B) exhibit the achieved resolution in the NN channel at incident energies of 94.1 and 159.1 MeV, respectively. Because of the extremely low nuclear cross section for the first excited state in xenon, the energy slits were opened. The resolution at lower energy with the wider energy slits was only 250 keV FWHM, whereas at $T_p = 159.1$ MeV with tight slits it was 280 keV FWHM. All quoted resolutions

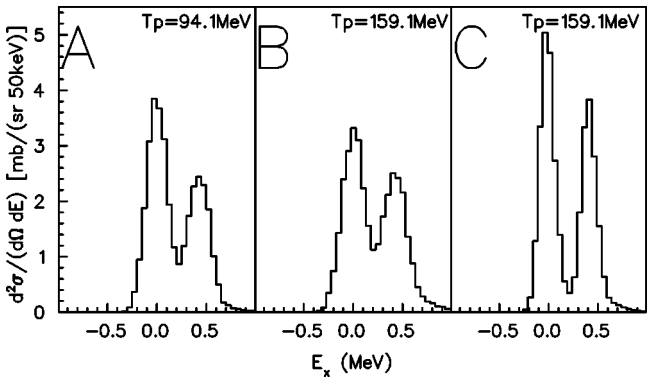


FIG. 1. Zero-degree excitation spectra for the $^{7}$Li$(p,n)^{7}$Be reaction obtained at (A) $T_p=94.1$ MeV, (B) and (C) at $T_p=159.1$ MeV. The two states in $^{7}$Be are the g.s. and first excited state at 0.429 MeV. The resolutions obtained with a ''Gaussian plus a tail'' fit were FWHM = 250 keV for (A) and FWHM = 280 keV for (B). Both spectra in (A) and (B) were generated using the NN channel. Panel (C) displays spectrum obtained also at $T_p$ = 159.1 MeV, but with the NP channel (see text). In this case the resolution was FWHM = 180 keV.

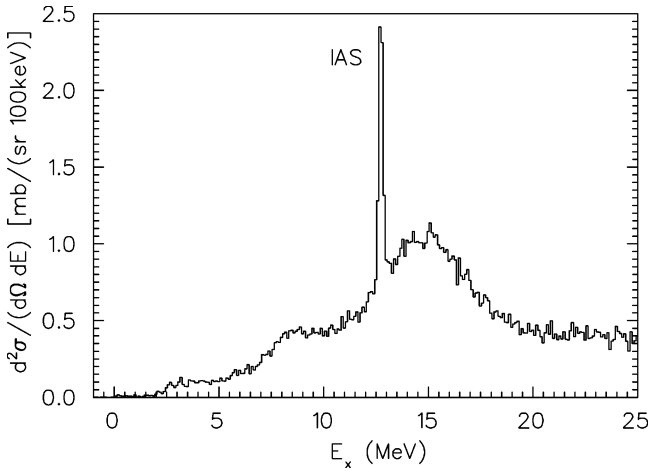


FIG. 2. Zero-degree $^{127}$Xe excitation energy spectrum obtained at $T_p=159.1$ MeV. The dominant feature in the spectra is the isobaric analog transition (Fermi transition) at $E_x=12.68$ MeV. The spectrum is binned with 100 keV per channel.

were determined using the $^{7}$Li$(p,n)^{7}$Be reaction (as displayed in Fig. 1). At medium energy we were able to make use of the more efficient NP channel and hence could run with a lower beam current. The NN channel at this energy was used to provide only the overall normalization. Figure 1(C) displays one of two different cuts, optimized for this experiment in the NP channel. A resolution of about 180 keV FWHM at $T_p=159.1$ MeV was achieved. At the high input energy (from the NP channel) the resolution was only 330 keV FWHM. More details about optimizing INPOL and its triggers for a high resolution measurement can be found in Ref. [12]. The production spectra will always represent a sum of all ''good events.'' Therefore, one can expect the final resolution in the $^{127}$Xe spectra to be slightly worse than values cited above, which were obtained in single short runs.

We have analyzed spectra obtained from the NP channel at medium energy and from the NN channel at the low energy. At 159.1 MeV incident proton energy and assuming that the zero-degree cross section is a measure of GT strength, we have obtained the GT strength up to 20 MeV excitation in $^{127}$Xe. At both lower incident energies a closer look is taken at the first excited state and we present a comparison of both excitation spectra up to the particle emission threshold. It will be shown that the zero-degree differential cross section for the first excited state follows the energy dependence of a GT transition. The data taken at high input energy will be used only to discuss the spectrum shape.

### B. Experimental results

The final spectra are corrected for neutron detector efficiencies and neutron absorption in the air and other material in the 159 m flight path. The combined corrections were determined as a function of energy by measuring the $^{7}$Li$(p,n)^{7}$Be spectrum at incident proton energies of 94, 104, 159, and 197 MeV. The $^{7}$Li$(p,n)^{7}$Be(g.s. $+0.429$ MeV) reaction has been measured over a range of energies from 80 to 800 MeV [14]. From that reference we use the c.m. cross section of $(26.0\pm0.8)$ mb/sr as constant over the energy range of this experiment. This calibrates our neutron detectors efficiency to a systematic error of less than 2%.

In the NN channel the normalization varied by about 20% between the lowest and the highest energy used in this experiment. The NP channel cannot be used for energies below about 120 MeV. Thus, the 104 and 94 MeV $^{7}$Li$(p,n)$ data do not provide a low energy calibration point in the NP channel for the $T_p=159.1$ MeV runs. Instead, the NP channel in the region of the $^{127}$Xe IAS was calibrated with the value of the differential cross section for the $^{12}$C$(p,n)^{12}$N(g.s.) transition measured in the NN channel. The g.s. $Q$ value is $-18.1$ MeV; so the neutron energy for this transition is lower than the energy for neutrons in the region of the $^{127}$I$(p,n)$ IAS transition.

The cross section uncertainties cited in this paper are statistical. An independent study has shown [15] that uncertainties in target thicknesses may contribute systematic errors up to 5%.

The $^{127}$I target was prepared as a $^{40}CaI_2$ (99% enriched in $^{40}$Ca) composite with a binder containing primarily $^{12}$C and $^{1}$H. The target thickness was 29.5 mg/cm$^2$. Both $^{40}$Ca and $^{12}$C have negative $Q$ values large enough to place the contaminant events at lower neutron energies than the IAS in xenon. Nevertheless, at the time of the experiment data were taken on background targets and all contaminant contributions have been carefully subtracted.

Data taken with $^{12,13}$C and $^{26}$Mg targets helped to obtain the exact input energy needed to determine the excitation energy of the IAS in xenon, which was previously not known.

Double-differential cross sections from the $^{127}$I$(p,n)^{127}$Xe reaction at $\theta=0°$ and $T_p=159.1$ MeV are displayed in Fig. 2 as a function of excitation energy up to $E_x=25$ MeV. The spectrum is dominated by the IAS (Fermi) peak. The visible peaks in Fig. 2 (or see the inset in Fig. 8) at $E_x=2.62\pm0.05$ and $E_x=3.08\pm0.05$ MeV correspond to a possible group of GT states in $^{127}$Xe not listed in Ref. [10]. The IAS is riding on a broad GT resonance centered around $E_x=14.5$ MeV. Assuming a smooth shape of

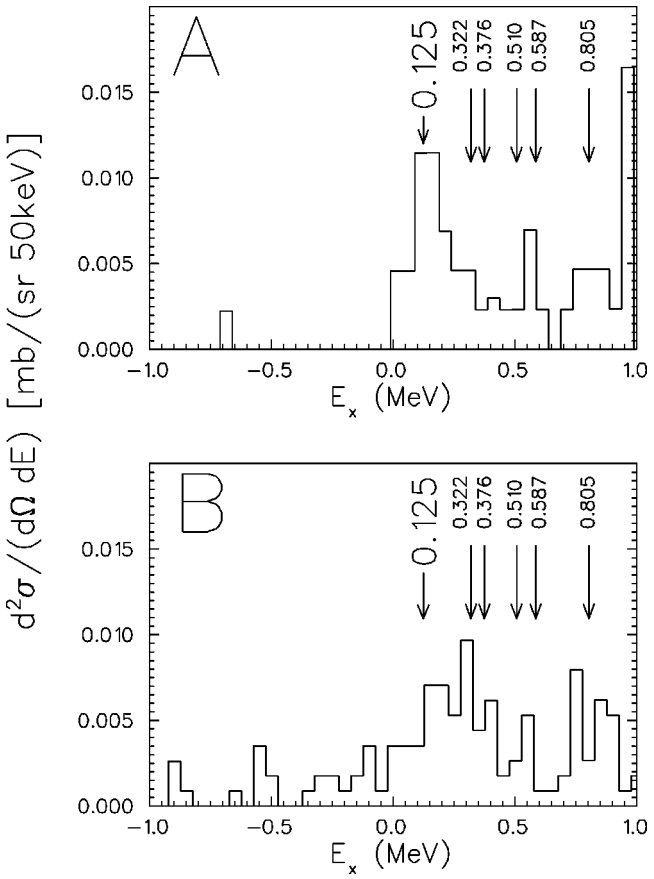


FIG. 3. Comparison of zero-degree $^{127}$Xe spectra up to 1.0 MeV excitation energy in $^{127}$Xe obtained at (A) $T_p=159.1$ MeV using the NP channel and at (B) $T_p=94.1$ MeV using the NN channel. The arrows indicate expected positions for the first excited state at 0.125 MeV and other $(3/2)^+$ and $(5/2)^+$ GT transitions up to 900 keV excitation energy [10]. The expected excitation energy of these states is given in MeV. In (A) the first excited state in $^{127}$Xe is close to the predicted position at $E_x=0.125$ MeV. In (B), the excitation of this state is still visible. At both energies, there is evidence for the excitation of the $(5/2)^+$, 805 keV state.

the GT resonance underneath the IAS and Gaussian shape of the IAS, the IAS position has been determined to be $E_x(\mathrm{IAS})=(12.68\pm0.05)$ MeV and the associated cross section $\sigma_{\mathrm{IAS}}=(4.29\pm0.12)$ mb/sr. To calculate the excitation energy nuclear masses from Ref. [16] were used. The fit also yields a $\mathrm{FWHM}_{\mathrm{IAS}}=213$ keV. The measured Coulomb displacement energy is $\Delta E_c=(14.13\pm0.05)$ MeV.

Figure 3 presents a comparison of the zero-degree spectra for the $^{127}\mathrm{I}(p,n)^{127}\mathrm{Xe}$ reaction at 159.1 MeV (top panel) and at 94.1 MeV (bottom panel) in the vicinity of the first excited state. The fit to the IAS's (not shown in the figure) yielded FWHM = 193 keV for Fig. 3(A) (where a slightly different cut has been used than in Fig. 2) and FWHM = 250 keV for Fig. 3(B). Because of the poor resolution in Fig. 3(B) the signal from the first excited state is weaker. At medium input energy one notes not only a superior energy resolution, but also a better background suppression. This is partially explained by different collection times and other conditions at both energies. The spectra shown in Fig. 3(A) and in Fig. 3(B) yield similar nuclear cross sections associated with the transition to the first excited state in the $^{127}\mathrm{I}(p,n)^{127}\mathrm{Xe}$ reaction at both incident energies. At $T_p=159.1$ MeV we measure $\sigma_{\mathrm{lab}}=(40.4\pm8.8)$ $\mu$b/sr and at $T_p=94.1$ MeV we measure $\sigma_{\mathrm{lab}}=(29.1\pm6.8)$ $\mu$b/sr. That these values are essentially the same within statistics is not surprising because of the slow energy dependence for GT type transitions in $(p,n)$ reactions at proton incident energies between 100 and 200 MeV [17].

Figure 4(A) presents a comparison of the zero-degree experimental double-differential cross sections in the laboratory for the $^{127}\mathrm{I}(p,n)^{127}\mathrm{Xe}$ reaction. Data at all three input energies superimposed are shown up to 15 MeV excitation energy in $^{127}$Xe. The position of the expected particle emission threshold (PET) for this nucleus ($E_x=7.223$ MeV) is marked with an arrow. The dashed line displays data collected at low incident energy. The data obtained at medium and high energies (displayed as solid histograms) agree in shape remarkably well. Figure 4(B) presents the data obtained at low and medium energies in 0–10 MeV excitation energy. It is clear that with increasing excitation energy, the two spectra begin to differ in shape and magnitude up to a factor of 2 around 10 MeV excitation. Figures 4(C), 4(D), and 4(E) show the expanded region of the IAS at the three incident energies: (C) at 94.1 MeV, (D) at 159.1 MeV, and (E) at 197.4 MeV. One can see a dramatic change in the IAS strength between Fig. 4(D) and Fig. 4(E), which agrees with the well-known energy dependence for this type of transition [13]. However, the cross section for the IAS transition in Fig. 4(C) at 94.1 MeV is smaller than that expected based on distorted-wave impulse approximation (DWIA) calculations employing standard effective interactions and optical-model potentials. This and the difference in the overall shape of the spectrum at low energy when compared to the shape observed at both higher energies suggests that distortion effects for this target nucleus at this energy are stronger than those predicted by the global optical-model parameters. As mentioned before, data were also taken for the $^{26}\mathrm{Mg}(p,n)^{26}\mathrm{Al}$ reaction at both lower energies. In the latter case the IAS yields were consistent with the expected energy dependence. The difference in the shape generated by the $^{127}\mathrm{I}(p,n)$ reaction at 94.1 MeV compared to both higher input energies will be described in more detail in the next section.

## III. EXTRACTION OF THE GT STRENGTH

It has been shown [13] that the zero-degree $(p,n)$ cross section can be parametrized as

$$\sigma=\hat{\sigma}_{\alpha}(E_p,A)F(q,\omega)B(\alpha), \tag{2}$$

where $\hat{\sigma}_{\alpha}$ is the specific unit cross section, $B(\alpha)$ the matrix element for the given transition and $\alpha$=F or GT. The function $F(q,\omega)$ is used to extrapolate the measured GT($F$) cross section at the empirical $(q,\omega)$ values to the values at $q=\omega=0$. The function $F(q,\omega)$ is equal to unity at $q=\omega=0$. This provides a very useful proportionality between $(p,n)$ cross sections and allowed beta-decay transition strengths, $B(\alpha)$. In practice, the measured cross section to an excited state representing a GT transition at the physical momentum transfer $q$, and energy loss $\omega$ must be corrected with the above function to values at $q=\omega=0$ [13].

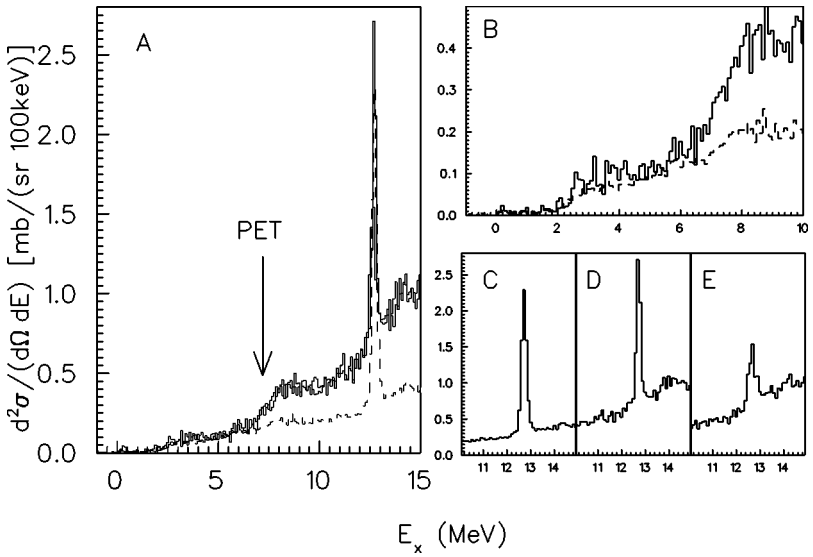


FIG. 4. (A) Zero-degree double differential cross sections for the $^{127}$I$(p,n)^{127}$Xe reaction up to 15.0 MeV excitation energy for all three incident energies superimposed. In (A) the dashed histogram displays data obtained at $T_p = 94.1$ MeV and the solid histograms represent data obtained at $T_p = 159.1$ MeV and $T_p = 197.4$ MeV. The arrow indicates the energy location corresponding to particle emission threshold (PET). Panel (B) represents an expanded energy range 0–10 MeV for data obtained at 159.1 MeV (solid line) and at 94.1 MeV (dashed line). The peaks visible between 2 and 4 MeV have excitation energies of 2.7 and 3.1 MeV. Panels (C), (D), and (E) represent the IAS region obtained at 94.1, 159.1, and 197.4 MeV incident energies, respectively.

Evaluations of the $F(q,\omega)$ functions were done at 94.1 and 159.1 MeV with microscopic DWIA calculations using the computer code DW81 [18]. Three basic ingredients are required by the code: nucleon-nucleon interaction, nuclear structure, and distorted-wave parametrization. The free nucleon-nucleon interaction as parametrized by Franey and Love [19] for the interaction between the incident and struck nucleons was used. Particle-hole transitions between $2d,1g$, and $1h$ shell model states [20–22] were assumed to be the major components for positive parity transitions up to the analog state. Harmonic oscillator wave functions were assumed for the single-particle states. Distorted waves for incident and outgoing nucleons were calculated using the optical-model potential parameters obtained by Schwandt *et al.*, for medium mass nuclei in the energy range 80–200 MeV [23]. The values obtained for $F(q,\omega)$ at 159.1 MeV were quite insensitive to the assumed particle-hole transition densities, to within a few percent. However, the same was not true at 94.1 MeV. The values for $F(q,\omega)$ function for transitions up to 10 MeV excitation energy were within 10% but deviated by as much as 50% with increasing excitation energy. The predicted strong energy dependence of the $F(q,\omega)$ at low incident energy reflects the difference in the experimental shape of the spectra as shown in Fig. 4(B). Therefore the calibration of the GT strength at 94.1 MeV incident energy depends on the assumed $F(q,\omega)$ function and is model dependent.

To obtain the GT strength from the measured cross sections, allowed beta-decay information for a given transition in the same nucleus is used [24]. When this information is not available, the ratio of unit GT and $F$ cross sections parametrized by Eq. (1) must be employed. In that equation $E_0$ is an empirical constant which for even-even nuclei has been evaluated to be $(55 \pm 1.7)$ MeV [13]. The Fermi strength for the iodine nucleus is $B(\mathrm{F}) = (N-Z) = 21$ units. The zero-degree differential cross section for this transition corrected by the $F(q,\omega)$ function and divided by $B(F)$ is defined as $\hat{\sigma}_F$. The unit cross section $\hat{\sigma}_{\mathrm{GT}}$ is obtained using in Eq. (1) the above $\hat{\sigma}_F$ and $E_0$ values. To reflect the fact that for some odd nuclei smaller values of $E_0$ have been reported [24], a systematic error in $E_0 = (55^{+1.7}_{-10.0})$ MeV is assigned. The GT strength from the 159.1 MeV data was extracted using the above $\hat{\sigma}_{\mathrm{GT}}$, and the zero-degree differential cross section corrected with the DWIA calculated $F(q,\omega)$ function.

Figure 5 shows the predicted $F(q,\omega)$ energy dependence at 94.1 MeV incident energy (solid line) calculated for $1g$-$1g$ particle-hole configurations. This curve is also a good representation of the calculated $F(q,\omega)$ functions obtained with other particle-hole configurations. The strong energy dependence displayed at 94.1 MeV is not present in the calculations done at 159.1 MeV. As one can see in Fig. 5

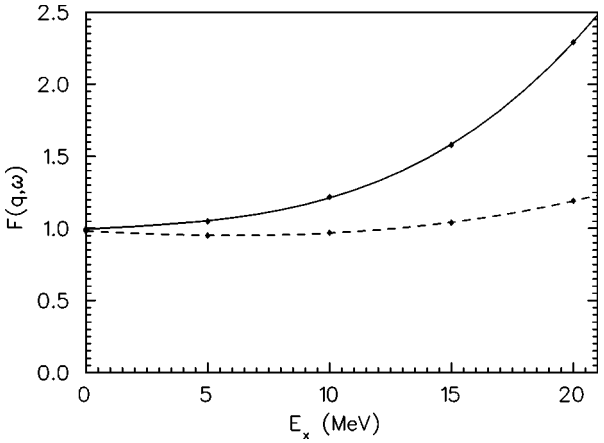


FIG. 5. Correction functions $F(q,\omega)$ obtained using DWIA calculations at $E_x = 0, 5, 10, 15, 20$, and 25 MeV assuming $1g$-$1g$ particle-hole configurations at $T_p = 94.1$ MeV (solid line) and at $T_p = 159.1$ MeV (dashed line).

TABLE I. Experimental double-differential cross sections and corresponding $B(\mathrm{GT})$ values for the $^{127}\mathrm{I}(p,n)^{127}\mathrm{Xe}$ reaction at $T_p = 159.1$ MeV and $\theta_{\mathrm{lab}} = 0\,°$. The step size is 0.5 MeV. The $B(\mathrm{GT})$ are expressed in unit GT. All errors are statistical only.

| Excitation (MeV) | mb/(sr MeV) | $B(\mathrm{GT})$ |
|---|---|---|
| 0.0–0.49 | 0.05±0.01 | 0.027±0.004 |
| 0.5–0.99 | 0.04±0.01 | 0.021±0.004 |
| 1.0–1.49 | 0.04±0.01 | 0.022±0.004 |
| 1.5–1.99 | 0.07±0.01 | 0.037±0.005 |
| 2.0–2.49 | 0.18±0.01 | 0.099±0.008 |
| 2.5–2.99 | 0.39±0.02 | 0.217±0.012 |
| 3.0–3.49 | 0.47±0.02 | 0.261±0.013 |
| 3.5–3.99 | 0.51±0.02 | 0.285±0.014 |
| 4.0–4.49 | 0.51±0.02 | 0.283±0.014 |
| 4.5–4.99 | 0.51±0.03 | 0.281±0.015 |
| 5.0–5.49 | 0.57±0.03 | 0.319±0.016 |
| 5.5–5.99 | 0.79±0.03 | 0.437±0.018 |
| 6.0–6.49 | 0.87±0.03 | 0.487±0.019 |
| 6.5–6.99 | 0.98±0.03 | 0.547±0.021 |
| 7.0–7.49 | 1.39±0.04 | 0.776±0.026 |
| 7.5–7.99 | 1.72±0.04 | 0.960±0.030 |
| 8.0–8.49 | 2.05±0.05 | 1.145±0.033 |
| 8.5–8.99 | 2.17±0.05 | 1.219±0.035 |
| 9.0–9.49 | 2.08±0.05 | 1.173±0.034 |
| 9.5–9.99 | 2.13±0.05 | 1.206±0.035 |
| 10.0–10.49 | 2.16±0.05 | 1.224±0.035 |
| 10.5–10.99 | 2.28±0.05 | 1.302±0.037 |
| 11.0–11.49 | 2.57±0.06 | 1.473±0.041 |
| 11.5–11.99 | 2.73±0.06 | 1.578±0.043 |
| 12.0–12.49 | 3.32±0.06 | 1.913±0.050 |
| 12.5–12.99 | 8.17±0.10 | 2.273±0.071 |
| 13.0–13.49 | 4.37±0.07 | 2.535±0.062 |
| 13.5–13.99 | 4.76±0.08 | 2.835±0.067 |
| 14.0–14.49 | 5.09±0.09 | 3.058±0.074 |
| 14.5–14.99 | 5.07±0.09 | 3.076±0.073 |
| 15.0–15.49 | 5.33±0.09 | 3.269±0.077 |
| 15.5–15.99 | 4.82±0.08 | 2.986±0.072 |
| 16.0–16.49 | 4.32±0.09 | 2.710±0.073 |
| 16.5–16.99 | 4.04±0.11 | 2.561±0.079 |
| 17.0–17.49 | 3.39±0.07 | 2.179±0.061 |
| 17.5–17.99 | 3.11±0.08 | 2.028±0.063 |
| 18.0–18.49 | 2.72±0.07 | 1.797±0.057 |
| 18.5–18.99 | 2.54±0.07 | 1.699±0.055 |
| 19.0–19.49 | 2.31±0.07 | 1.573±0.056 |
| 19.5–19.99 | 2.19±0.07 | 1.511±0.054 |

(dashed line), the $F(q,\omega)$ values at higher energy are close to unity up to about 20 MeV excitation energy. The cross section measured at 159.1 MeV for the IAS peak has a value of 4.29 mb/sr [$F(q,\omega)=1$ at $E_x=$IAS], which is used to obtain a $\hat{\sigma}_F = (0.20 \pm 0.01$ stat) mb/sr unit F. The value for the corresponding GT unit cross section is $\hat{\sigma}_{\mathrm{GT}} = (1.71 \pm 0.05\ \mathrm{stat}^{+0.09}_{-0.62}\mathrm{syst})$ mb/sr unit GT. This result is in good agreement with unit cross sections reported in Ref. [13] for nuclei in the same mass region at 160 MeV incident energy. In Table I we list the double-differential nuclear cross sections measured at medium energy and the calculated $B(\mathrm{GT})$

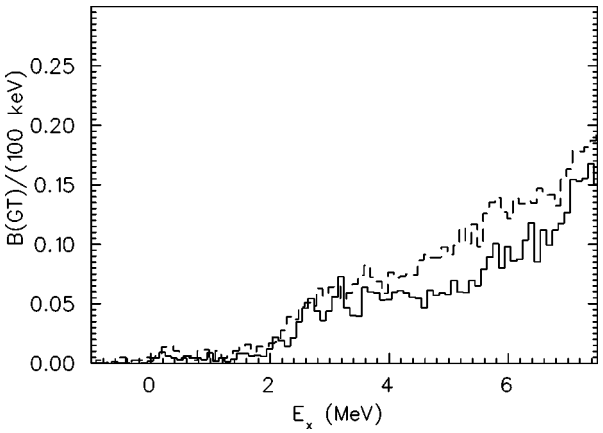


FIG. 6. Calculated $B(\mathrm{GT})$ values up to 7.5 MeV excitation (particle emission threshold) in $^{127}$Xe obtained from the $^{127}\mathrm{I}(p,n)^{127}\mathrm{Xe}$ reaction at 94.1 MeV (dashed histogram) and at 159.1 MeV (solid histogram) incident energies.

values per 0.5 MeV in the full covered range of excitation energy. The first excited state in $^{127}$Xe is estimated to have a $B(\mathrm{GT}) = (0.0232 \pm 0.004\ \mathrm{stat}^{+0.0013}_{-0.0084}\mathrm{syst})$.

In Fig. 6 we compare $B(\mathrm{GT})$ values deduced from the 94.1 and 159.1 MeV data only up to 7.223 MeV, the excitation energy in $^{127}$Xe above which particle emission occurs. The solid histogram displays data at 159.1 MeV, whereas the dashed histogram displays data at low incident energy. The integral from $E_x = 0$ up to the particle emission threshold for medium input energy is: $(3.67 \pm 0.05\ \mathrm{stat}^{+0.21}_{-1.34}\mathrm{syst})$ unit GT and for low input energy is $(5.03 \pm 0.07\ \mathrm{stat}^{+0.30}_{-1.83}\mathrm{syst})$ unit GT. The running sum of the $B(\mathrm{GT})$ strength obtained from the data at 159.1 MeV up to 20 MeV excitation is presented in Fig. 7. The total $B(\mathrm{GT})$ sum up to 20 MeV excitation is $(53.54 \pm 0.22\ \mathrm{stat}^{+3.32}_{-19.47}\mathrm{syst})$ unit GT.

Iodine is an odd nucleus and as such the IAS may be excited by a mixture of $\sigma_F$ and $\sigma_{\mathrm{GT}}$ cross sections. The data obtained at all three incident energies (94.1, 159.1, and 197.4 MeV) may be used to estimate if there is any sizable admixture of GT ($\Delta J = 1$) in the excitation of the IAS. Such an admixture becomes apparent by studying the ratio of the IAS to the surrounding background, which is assumed to be the

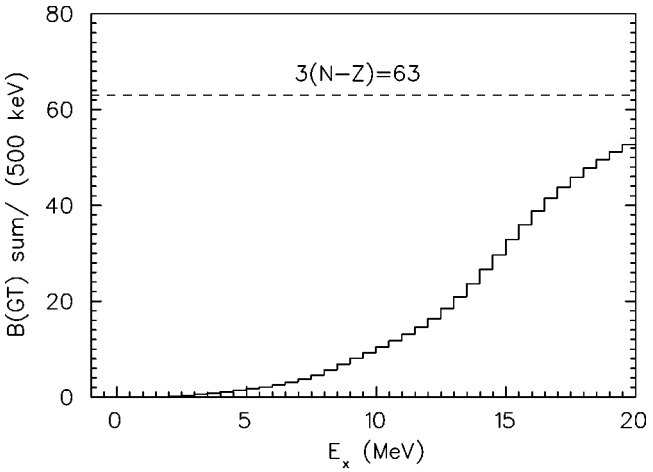


FIG. 7. Running sum of $B(\mathrm{GT})$ strength inferred from the $^{127}\mathrm{I}(p,n)^{127}\mathrm{Xe}$ reaction at 159.1 MeV.

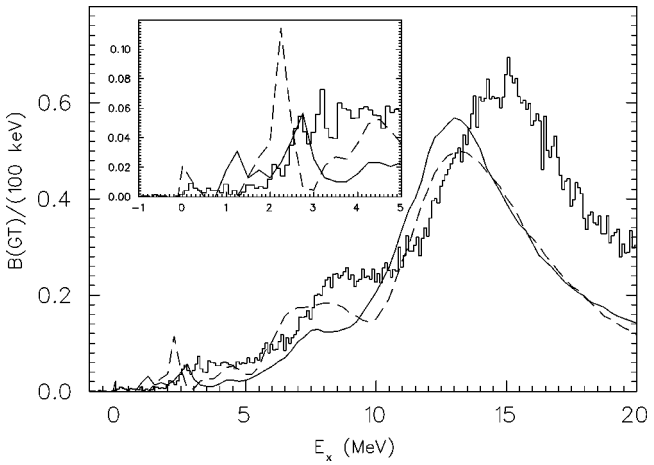


FIG. 8. $B$(GT) vs excitation energy in $^{127}$Xe per 100 keV shown as a histogram plot at $T_p = 159.1$ MeV. Also displayed is the comparison of the data to two theoretical evaluations of the $B$(GT) strength in $^{127}$Xe. The dashed line are results reported in Ref. [21] and the solid line are results from Ref. [22]. The inset represents an expanded energy range up to 5 MeV excitation.

giant GT resonance, as a function of incident energy. In the present case, the ratio behaves in the manner expected from Ref. [13] for Fermi to GT cross section; so within error bars we conclude that there is no more than about 5% GT strength in the IAS peak.

## IV. THEORETICAL EVALUATIONS OF $B$(GT)

The GT strength function inferred from the zero-degree $^{127}$I$(p,n)^{127}$Xe reaction at 159.1 MeV is shown in Fig. 8 as a histogram plot. This is the first GT strength function for the $^{127}$Xe extracted up to 20 MeV. As mentioned before, it assumes that the zero-degree $(p,n)$ cross section at this bombarding energy is dominated by the $L=0$ component, the GT contribution to the excitation of the IAS may be neglected, and the IAS peak is above a smooth GT continuum of states. Those assumptions have been successfully explored in other cases, for instance, Ref. [25]. The obtained empirical GT strength function is compared below to the available theoretical predictions.

In his paper, Haxton [1] extrapolated from empirical $(p,n)$ results on $^{98}$Mo and $^{71}$Ga to estimate the $^8$B neutrino absorption cross section on $^{127}$I. In 1991, Engel, Pittel, and Vogel [20] reported on a calculation using a configuration-mixing quasiparticle Tamm-Dancoff approximation to obtain the expected event rate for the $^{127}$I detector. The same authors reported on an improved calculation [21] which resulted in a larger $^8$B neutrino absorption cross section than in their earlier work.

Figure 8 compares our $B$(GT) strength function (shown as a histogram) to the reported calculated Gamow-Teller distribution in unit GT up to 20 MeV excitation (as a dashed line). Figure 8 shows that the calculation (dashed line) is smaller by about 15% in magnitude and locates the peak of the broad GT resonance at a lower energy. The calculation is shifted by almost 2 MeV from the observed maximum. Also the strong calculated GT excitation near 2.4 MeV is not confirmed by the present measurement.

Using the theory of finite Fermi systems, Lutotansky and Shul'gina [22] also report on calculated values for solar neutrino cross section for the $^{127}$I detector. Their results in unit GT are presented in Fig. 8 (solid line) and are compared to the empirical $B$(GT) strength function and to the results from Ref. [21]. Their predictions are similar to those of Ref. [21]. Both calculations place the peak of the giant GT resonance about 2 MeV below the observed value. At lower excitation the calculations appear to be in relatively good agreement in terms of position and strength with the peak near 2.8 MeV. However, predicted excitations below that peak in the range 1–2 MeV seem to be either missing or have a much smaller strength (see inset in Fig. 8).

As shown in Fig. 7 the sum $B$(GT) up to 20 MeV excitation energy in $^{127}$Xe has a value of (53.54 $\pm 0.22$ stat$^{+3.32}_{-19.47}$syst) unit GT, which is $(85^{+5.27}_{-30.9}$syst)% of the $3(N-Z)=63$. The authors in Refs. [21,22] have assumed quenchings of 63% and 64%, respectively. The summed strengths up to 20 MeV are 39.8 unit GT from Ref. [21] and 39.9 unit GT from Ref. [22]. Our experiment yields 53.5 unit GT.

TABLE II. Comparison of sensitivities to $^7$Be and $^8$B solar neutrinos between $^{127}$I and $^{37}$Cl detectors. The total cross sections are in units of $10^{-45}$ cm$^2$.

| | $^{127}$I | $^{37}$Cl |
|---|---|---|
| $^7$Be | $1.22 \pm 0.40$ | $0.24 \pm 0.02$ |
| $^8$B | $(4.3 \pm 0.6) \times 10^3$ | $(1.11 \pm 0.08) \times 10^3$ |
| Ratio $^8$B/$^7$Be | $3525 \pm 1260$ | $4625 \pm 510$ |

## V. SENSITIVITY OF $^{127}$I TO $^7$Be AND $^8$B NEUTRINOS

The $^7$Be solar neutrino capture cross section in $^{127}$I may be estimated by using Eq. (1) in Haxton's paper [1]. In what follows only statistical uncertainties will be used. The empirical value $B(\mathrm{GT}) = (0.0234 \pm 0.005)$ for the $5/2^+ \rightarrow 3/2^+$ transition to the 0.125 MeV excited state translates into a $\log(ft) = 5.2 \pm 0.2$. We have used values from Ref. [24] for the constants relating $B$(GT) and $ft$. This indicates a neutrino capture cross section $\sigma(^7\mathrm{Be}) = (1.22 \pm 0.4) \times 10^{-45}$ cm$^2$. This $^7$Be neutrino capture cross section for $^{127}$I is approximately 5.1 times that for these neutrinos by $^{37}$Cl where the latter cross section is obtained from the ground state to ground state decay rate of $^{37}$Ar to $^{37}$Cl.

The $^8$B solar neutrino capture cross section in $^{127}$I up to particle emission threshold may be estimated from the empirical $B$(GT) strength function and from knowledge of the $^8$B neutrino spectrum. This has been done by Haxton [26], yielding a value of $(4.3 \pm 0.6) \times 10^{-42}$ cm$^2$ or about 3.9 times that for $^8$B neutrinos on $^{37}$Cl. In Table II we compare the cross sections of $^{127}$I and $^{37}$Cl detectors for $^7$Be and $^8$B solar neutrinos. We use the most recent solar neutrino fluxes of Bahcall, Basu, and Pinsonneault [27] to estimate (30.6 $\pm 5.3$) SNU (solar neutrino unit, 1 SNU$=10^{-36}$ interactions per target atom per second) as the total predicted detection rate of solar neutrinos by $^{127}$I. This detection rate can be compared with the corresponding one for $^{37}$Cl of (7.7 $\pm 1.1$) SNU. To the above cross sections for $^7$Be and $^8$B and additional estimated contributions of 0.37 SNU and 1.32 SNU from the solar neutrino continuous sources $^{13}$N and $^{15}$O and 0.84 SNU from the solar neutrino discrete source *pep* have been included [27].

The $B(\mathrm{GT})$ for the first excited state in $^{127}$Xe represent a small GT strength and as such the normalization of the measured differential $(p,n)$ cross section in unit GT has been questioned. It has been argued by Austin *et al.* [28] and more recently by Haxton [29] that for weak transitions whose GT strengths represent a small fraction of the sum rule limit, the $(p,n)$-based results might not represent $\beta$-decay $B(\mathrm{GT})$ values. This possibility will be tested by the forthcoming $^{37}$Ar source neutrino calibration. The threshold for the $^{127}$I to $^{127}$Xe transition, $Q=-789$ keV, permits direct calibration of this transition with an intense source of $^{37}$Ar, 814 keV neutrinos. As indicated before, the production of a MCi source of $^{37}$Ar in the BN-600 fast neutron reactor is now beginning in Russia [3]. The $^{37}$Ar source will be produced via the $^{40}\mathrm{Ca}(n,\alpha)^{37}\mathrm{Ar}$ reaction. The comparison of the directly measured neutrino cross section with the one presented here from the $(p,n)$-determined $B(\mathrm{GT})$ will provide a direct test of the applicability of the $B(\mathrm{GT})$-derived neutrino cross sections.

## VI. CONCLUSIONS

In this paper we present clear evidence for the excitation of the 0.125 MeV state in $^{127}$Xe observed at two incident energies in the $(p,n)$ reaction at $\theta_{\mathrm{lab}}=0\,^{\circ}$. We have reported the nuclear cross section and the $B(\mathrm{GT})$ value for this transition. We have extracted the GT strength function for this nucleus up to 20 MeV excitation. The integral up to particle emission threshold yields $(3.67\pm0.05\ \mathrm{stat}^{+0.21}_{-1.34}\mathrm{syst})$ unit GT. This seems to be in good agreement with the $B(\mathrm{GT})$ value of $3.2\pm0.65$ reported in Ref. [11]. The present $B(\mathrm{GT})$ for the 0.125 MeV state is higher than the value estimated in Ref. [11], which is easily explained by the better energy resolution in these data ($\Delta E=193$ keV). From our measurement we learned that most of the GT strength near $E_x=0$ MeV is located in the excitation of the first excited state in $^{127}$Xe. We have also reported for the first time the position of the IAS peak in $^{127}$Xe as well as a value for the Coulomb displacement energy.

We have compared the experimental GT strength function to available calculations. The empirical peak location of the giant GT resonance is near $E_x=14.5$ MeV, a value about 2 MeV higher than the models predict [21,22]. However, the overall shape of the GT resonances seems to be in fair agreement.

Measured $B(\mathrm{GT})$ for $^{127}$I neutrino detector sensitivity to the $^{7}$Be neutrinos yields a neutrino capture cross section of $\sigma(^{7}\mathrm{Be})=(1.22\pm0.4)\times10^{-45}$ cm$^2$. This value seems to be in reasonable agreement with theoretical predictions, which range from $0.7\times10^{-45}$ cm$^2$ to $2.2\times10^{-45}$ cm$^2$.

## ACKNOWLEDGMENTS

The authors would like to acknowledge the careful work done by Bill Lozowski in preparing the targets used in these runs, and also the crew of the IUCF Cyclotron. We also would like to thank Wick Haxton for calculating the $^{8}$B solar neutrino capture cross sections in $^{127}$I. This work was supported in part by NSF.

[1] W. C. Haxton, Phys. Rev. Lett. **60**, 768 (1988).
[2] B. T. Cleveland, T. Daily, R. Davis, Jr., J. Distel, K. Lande, C. K. Lee, P. Wildenhain, and J. Ulman, Astrophys. J. **495**, 505 (1998).
[3] K. Lande (unpublished).
[4] B. T. Cleveland *et al.*, in *Proceedings of the 23rd International Cosmic Ray Conference*, edited by D. A. Leahy, R. B. Hicks, and D. Venkatesan (University of Calgary, Alberta, Canada, 1993), Vol. 3, p. 865.
[5] G. Audi and A. H. Wapstra, Nucl. Phys. **A565**, 1 (1993).
[6] M. B. Aufderheide, S. D. Bloom, D. A. Resler, and C. D. Goodman, Phys. Rev. C **49**, 678 (1994).
[7] D. Krofcheck, E. Sugarbaker, J. Rapaport, D. Wang, J. N. Bahcall, R. C. Byrd, C. C. Foster, C. D. Goodman, I. J. Van Heerden, C. Gaarde, J. S. Larsen, D. J. Horen, and T. N. Taddeucci, Phys. Rev. Lett. **55**, 1051 (1985).
[8] A. E. Champagne, R. T. Kouzes, A. B. McDonald, M. M. Lowry, D. R. Benton, K. P. Coulter, and Z. Q. Mao, Phys. Rev. C **39**, 248 (1989).
[9] T. Lonnroth, J. Kumpulainen, and C. Tuokko, Phys. Scr. **27**, 228 (1983).
[10] K. Kitao and M. Oshima, Nucl. Data Sheets **77**, 1 (1996).
[11] E. Sugarbaker, in *G-T and Neutrino Cross Section Workshop Proceedings*, edited by K. Lande and P. Wildenhain (University of Pennsylvania, Philadelphia, 1993).
[12] M. Palarczyk *et al.*, Nucl. Instum. Methods Phys. Res. A (to be published).
[13] T. N. Taddeucci, C. A. Goulding, T. A. Carey, R. C. Byrd, C. D. Goodman, C. Gaarde, J. Larsen, D. Horen, J. Rapaport, and E. Sugarbaker, Nucl. Phys. **A469**, 125 (1987).
[14] T. N. Taddeucci, W. P. Alford, M. Barlett, R. C. Byrd, T. A. Carey, D. E. Ciskowski, C. C. Foster, C. Gaarde, C. D. Goodman, C. A. Goulding, E. Gülmez, W. Huang, D. J. Horen, J. Larsen, D. Marchlenski, J. B. McClelland, D. Prout, J. Rapaport, L. J. Rybarcyk, and W. C. Sailor, Phys. Rev. C **41**, 2548 (1990).
[15] M. Palarczyk (unpublished).
[16] A. H. Wapstra, Nucl. Phys. **A423**, 1 (1985).
[17] E. Sugarbaker, D. Marchlenski, T. N. Taddeucci, L. J. Rybarcyk, J. B. McClelland, T. A. Carey, R. C. Byrd, C. D. Goodman, W. Huang, J. Rapaport, D. Mercer, D. Prout, W. P. Alford, E. Gülmez, C. A. Whitten, and D. Ciskowski, Phys. Rev. Lett. **65**, 551 (1990).
[18] R. Schaeffer and J. Raynal, computer program DWBA70, 1970 (unpublished); J. R. Comfort, extended version DW81 1981 (unpublished).
[19] M. A. Franey and W. G. Love, Phys. Rev. C **31**, 488 (1985).
[20] J. Engel, S. Pittel, and P. Vogel, Phys. Rev. Lett. **67**, 426 (1991).

[21] J. Engel, S. Pittel, and P. Vogel, Phys. Rev. C **50**, 1702 (1994).
[22] Yu. S. Lutotansky and N. B. Shul'gina, Phys. Rev. Lett. **67**, 430 (1991).
[23] P. Schwandt, H. O. Meyer, W. W. Jacobs, A. D. Bacher, S. E. Vigdor, M. D. Kaitchuck, and T. R. Donoghue, Phys. Rev. C **26**, 55 (1982).
[24] J. Rapaport and E. Sugarbaker, Annu. Rev. Nucl. Sci. **44**, 109 (1994).
[25] J. Rapaport, T. Taddeucci, T. P. Welch, C. Gaarde, J. Larsen, D. J. Horen, E. Sugarbaker, P. Koncz, C. C. Foster, C. D. Goodman, C. A. Goulding, and T. Masterson, Nucl. Phys. **A410**, 371 (1983).
[26] W. Haxton (private communication).
[27] J. N. Bahcall, S. Basu, and M. H. Pinsonneault, Phys. Lett. B **433**, 1 (1998).
[28] S. M. Austin, N. Anantaraman, and W. G. Love, Phys. Rev. Lett. **73**, 30 (1994).
[29] W. Haxton, Phys. Lett. B **431**, 110 (1998).